PTEP

Prog. Theor. Exp. Phys. **2023** 033J01(13 pages)
DOI: 10.1093/ptep/ptad030

Controllable electron self-injection in laser wakefield acceleration with asymmetric gas-jet nozzle

Zhenzhe Lei[1,2,3,⋆], Zhan Jin[1,2,3], Alexei Zhidkov[1,2], Naveen Pathak[1,2], Yoshio Mizuta[1,2], Kai Huang[2,4], Nobuhiki Nakanii[4], Izuru Daito[4], Masaki Kando[2,4], and Tomonao Hosokai[1,2,3]

[1]*SANKEN, Osaka University, Mihogaoka 8-1, Ibaraki, Osaka 567-0047, Japan*
[2]*Laser Accelerator R&D, Innovative Light Sources Division, RIKEN SPring-8 Center, Kouto 1-1-1, Sayo-cho, Sayo-gun, Hyogo 679-5148, Japan*
[3]*Gradurate School of Science, Osaka University, 1-1 Machikaneyama, Toyonaka 560-0043, Osaka, Japan*
[4]*Department of Advanced Photon Research, Kansai Photon Science Institute, National Institutes for Quantum Science and Technology, 8-1-7 Umemidai, Kizugawa, Kyoto 619-0215, Japan*
⋆E-mail: zlei25@sanken.osaka-u.ac.jp

Received October 3, 2022; Revised February 21, 2023; Accepted March 1, 2023; Published March 2, 2023

Beam charge control in the staging of laser wakefield acceleration (LWFA) is a crucial technique for developing full-optical jitter-free high-energy electron accelerators. Precise control of total charge in pre-accelerated electron bunches is necessary to achieve practical electron beam characteristics in the final acceleration stage(s). In contrast to the well-known cathode techniques in conventional accelerators, in LWFA the electron injection results from non-linear processes originating from plasma wave breaking. Therefore, the development of charge control requires a deep understanding of the electron self-injection processes and applications of non-trivial tools. The use of asymmetric gas-jet nozzles seems to be a promising way in developing charge control via tuning the target parameters such as plasma density, density slope, and acceleration length. Here, we demonstrate and characterize controllable electron self-injection, owing to a parametric resonance in slantwise density gas jets irradiated by 50 TW femtosecond laser pulses. The measured characteristics of the electron bunches, in which charge and energy distribution depend on the gas density and gas density gradient, agree well with those obtained by multidimensional particle-in-cell simulation and confirm the possibility of charge control.

Subject Index J27 (particle acceleration for plasma physics)

1. Introduction

Recent progress in the investigation of the laser wakefield acceleration (LWFA) technique opens ways to develop and elaborate laser-plasma electron accelerators [1–5]. Such accelerators, being jitter-free, may fill a certain niche in the acceleration family. So far, one of the main goals in LWFA research is the achievement of the highest energy of the accelerated electrons. In Ref. [6] over 8 GeV energy of accelerated electrons is reported for the discharged capillary target. Such an energy range is already of practical interest. However, accelerators require several other parameters and characteristics such as low energy spread, low emittance, low divergence, high charge density, stability, reproducibility and long operation time. LWFA techniques to match the performance of accelerators have yet to be studied in more depth.

Beam charge density control is a key part of acceleration systems. Thermal and photocathodes along with electron extraction techniques [7] provide the linear procedures that allow quite

precise control of electron bunch charges upon varying cathode temperature or laser pulse energy for further acceleration. In full optical LWFA, cathodes are formed via non-linear plasma processes such as longitudinal [8] and transverse [9] plasma wave breaking, ionization injection [10–12], parametric resonances [13] and others, which are very sensitive to plasma and laser pulse parameters. Similar to vacuum systems, LWFA can be subdivided conditionally into two parts: the electron injection and the electron acceleration, both for single and multiple stages acceleration techniques. The electron injection or cathode is a key part of the whole process responsible for the final charge, emittance and energy spread of the accelerated electrons [14].

Typically, plasma wave breaking, which results in the appearance of energetic electrons moving in the acceleration phase of the laser pulse wake, occurs in the vicinity of inhomogeneity of plasma electron density [15]. A monochromatic oscillation of plasma electrons here is impossible. With the decomposition of the wave, a proportion of electrons acquire momentum in the direction of laser propagation and velocities exceeding the phase velocity of the plasma wave. They are accelerated further. The relativistic wave breaking [16] has a different nature. Such a wave breaking is provoked when the electric field in the wave exceeds a certain threshold, typically equal to the "wave breaking limit" [17]. This process may occur even in uniform plasma. At moderate laser intensities, it limits the number of intact periods (buckets) of the wave in the wake. When the laser pulse intensity exceeds the threshold, only the first bucket, just behind the laser pulse, survives. Such processes are not easily controllable. It is clear that in the case of the relativistic wave breaking the injected charge will grow until its space charge locks the injection [18]. For a lower plasma field, wave breaking can be localized and therefore controlled with a steep density gradient [19] as well as in a certain position by (i) counter-propagating laser pulses [20], (ii) collision of a laser pulse and an electron beam, and (iii) parametric resonance [13]. With properly chosen parameters of plasma and laser pulses, such provocative wave breaking may give a controllable injection of plasma electrons allowing, along with slicing methods [21,22], to match the performance of conventional accelerator cathodes.

A gas target with density decreasing along the direction of laser pulse propagation has been shown to be of particular interest in the organization of controllable electron self-injection [19,23]. The application of gas targets with longitudinally varying density has also been considered as a way to increase the dephasing length in the LWFA [24]. The gas targets with negative density gradient have been numerically proposed for the controllable injection for gradient lengths comparable to the plasma wavelength [25–27]. Theoretical results have not demonstrated an essential difference in the final energy and charge distribution at chosen parameters. However, the first measurement with the use of two gas jets [28] resulting in non-uniform gas flux with the density gradient length far exceeding the plasma wavelength has demonstrated a clear dependency of the energy distribution of accelerated electrons on the plasma density profile. The low flexibility of the two gas-jet targets to tune the plasma parameters does not allow for easier control of the final electron bunches. It is clear that in a small density gradient target the main processes resulting in the wave breaking should be various parametric resonances.

In the present paper, we study LWFA in density ramp targets with small gradients to obtain controllable electron self-injection during the interaction of a femtosecond laser pulse with under-dense plasma. For that purpose, we developed a gas nozzle with a movable wall and a fixed length of 6 mm which provides a tunable negative gradient in the gas flux. Such a nozzle can provide three parameters: gas density, target length and density gradient. Here, we restricted our analysis to only the parameter of density gradient. Multidimensional particle-in-cell (PIC)

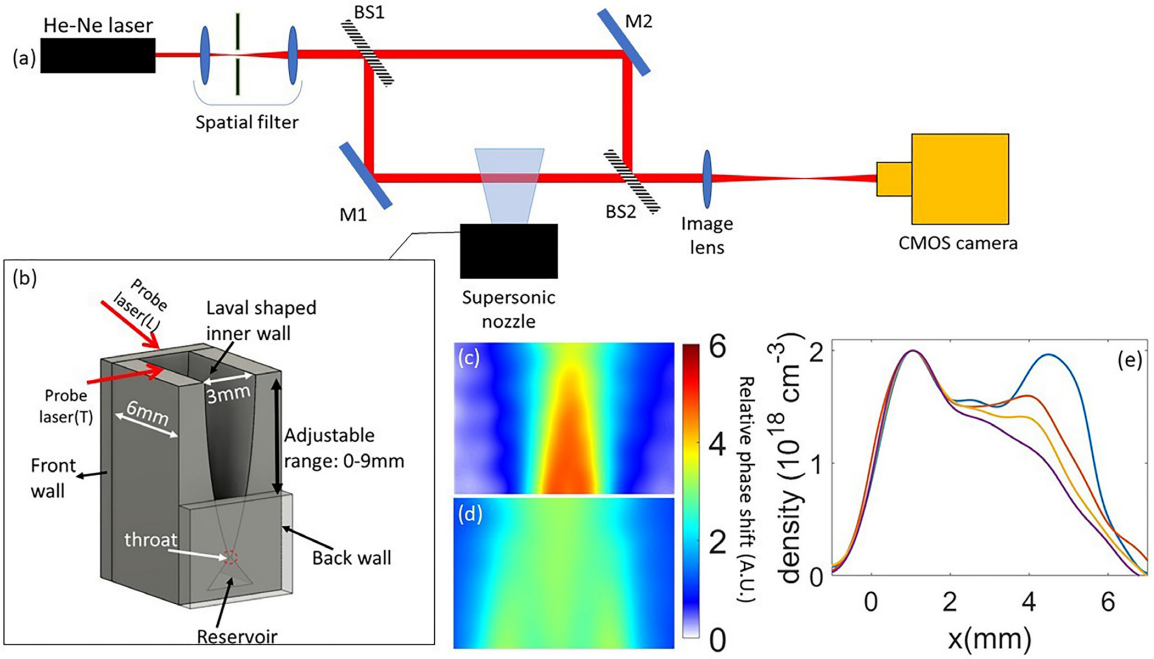

Fig. 1. (a) Schematic set up of Mach–Zehnder interferometer; (b) design of the asymmetric nozzle; (c) typical phase map of the asymmetric nozzle taken from 3 mm side [with probe laser (L)]; (d) typical phase map of the asymmetric nozzle taken from 6 mm side [with probe laser (T)]; (e) typical estimated neutral gas density profile for gas tank pressure at 0.5 Mpa along the 6 mm side for different back wall conditions: (blue line) back wall full close, (red line) back wall open for 5 mm, (yellow line) back wall open for 6 mm and (purple line) back wall open for 9 mm.

simulations are performed to reveal the mechanisms and processes of electron self-injection and electron acceleration in different negative density gradients.

2. Experimental setup

Gas density profiles of the gas jet were measured using the Mach–Zehnder interferometer (Fig. 1a). A continuous wave He-Ne laser (wavelength 633 nm) was used as a probe beam. A spatial filter was used to remove the aberrations and increase the laser beam diameter. The laser beam was split and rejoined using two beam splitters (BS1 and BS2, THORLABS). The gas-jet image was produced by an $f/10$ image lens ($f = 500$ mm) and picked up by a complementary metal-oxide-semiconductor (CMOS) camera (the IMAGEINGSOURS, DMK 33GP1300). The camera exposure time is set to the minimum, which equals 50 μs.

In this experiment, a specially designed slit nozzle for Mach 5 hydrogen flow with adjustable end walls was used to control the shape of the density ramp in a supersonic gas jet. The design of this nozzle is shown in the inset of Fig. 1(b). The nozzle slit had a width of 3 mm and a length of 6 mm. The transverse inner walls were made to a rapid expansion Laval shape [29,30] to avoid shockwaves in the supersonic gas flow. The front wall and back wall were flat with an adjustable height. Both front and back walls can move up to 9 mm down from the nozzle exit. The throat and reservoir are always covered so that gas can be choked inside the reservoir and there is no gas pressure drop inside the reservoir due to leakage. For this experiment, the front wall (entrance edge of the gas jet) was fully closed, and the back wall (exit of the gas jet) was adjusted to fine-tune the density ramp along the laser propagation direction. The gas jet

was driven by a fast solenoid valve (Smartshell Co. Ltd. A2-6443) which provides a pulsed jet with a rising time below 100 μs and a duration of 1.8 ms. A pressure controller (GE Druck PACE5000) was used to control the gas pressure of hydrogen (gas tank pressure) that was fed into the solenoid valve.

To obtain a detailed picture of this gas jet, the interferometry data was taken for both the 3 mm side [with probe laser (L)] and the 6 mm side [with probe laser (T)]. Figs. 1(c) and 1(d) show the typical phase map obtained from interferometry of the asymmetry nozzle from the 3 mm side and the 6 mm side, respectively. The neutral gas density was estimated using the same method as Ref. [31].The typical estimated neutral gas density for gas tank pressure 0.5 Mpa along the 6 mm side for different back wall conditions are shown in Fig. 1(e). The interferometry experiment was carried out with 3 Mpa nitrogen. Because the regulator for the hydrogen tank only allows operation below 0.5 Mpa, the fringe shift is invisible under such pressure. Since nitrogen and hydrogen have a similar ratio of specific heat (γ) at the same pressure and temperature [32], the nitrogen and hydrogen gas jets from this nozzle should have similar density profiles. When both walls were closed ($d = 0$ mm), the density showed a symmetric distribution with a rather flat distribution in the central region (blue line). When the back wall was fully open ($d = 9$ mm), the gas would leak into the vacuum in the absence of confinement. This induced a density drop at the end or exit of the gas jet and, therefore, a down-ramping distribution could be realized along the longitudinal axis, shown as the purple line. By controlling the height of the back wall ($d = 6$ mm, 5 mm), we were able to control the slope of the density down-ramp precisely (yellow and red line).

LWFA experiments were carried out with beamline 2 of Laser Acceleration Platform (LAPLACIAN) Ti: Sapphire laser system (Amplitude Technologies) at RIKEN SPring-8 Center based on a chirped pulse amplification (CPA) technique [33]. Beamline 2 delivers a 1.2 J laser pulse (on target) with a pulse duration of 24 fs and a peak power of 50 TW. The central wavelength of the laser system is 800 nm. The contrast ratio between the main pulse and the nanosecond pre-pulse caused by the amplified spontaneous emission (ASE) is better than 10^{-10}. The picosecond contrast was on the order of 10^{-6}–10^{-8}. The experimental setup is shown in Fig. 2. The laser pulses were focused on the front edge of the supersonic slit nozzle of a hydrogen gas jet by a gold-coated off-axis parabolic (OAP) mirror with $f/20$ ($f = 1500$ mm) via a dielectric-coated flat mirror. The focus spot size is about 24 μm in FWHM. The focused pulse on target intensity was estimated to be $\sim 10^{18}$ w cm^{-2}. The spatial distribution of the electron beams was measured by a movable phosphor screen (Mitsubishi Chemical Co. LTD, DRZ-High). The electron energy was measured by an electron spectrometer (ESM) with a magnetic field of 0.55 T and a length of 900 mm. The ESM was located 2.5 m away from the electron source. To obtain more accurate electron beam energy, the beam spatial measuring screen was moved away from the beam axis during the beam energy measurement. The same type of phosphor screen (DRZ-High) was also used in the ESM. The phosphor screen on ESM was covered by multilayers of metal foils, 50 μm of aluminium foils and 20 μm of titanium foil. Those metal foils protect the ESM screen from damage caused by background light from the intense laser pulse. Charged coupled device (CCD) cameras (Princeton Instruments, ProEM-HS: 1024BX3) were used to record the scintillating images.

The electron beam charge is evaluated from the ESM signal with the known sensitivity of the phosphor screen, quantum efficiency of the CCD camera, the efficiency of optics and the solid

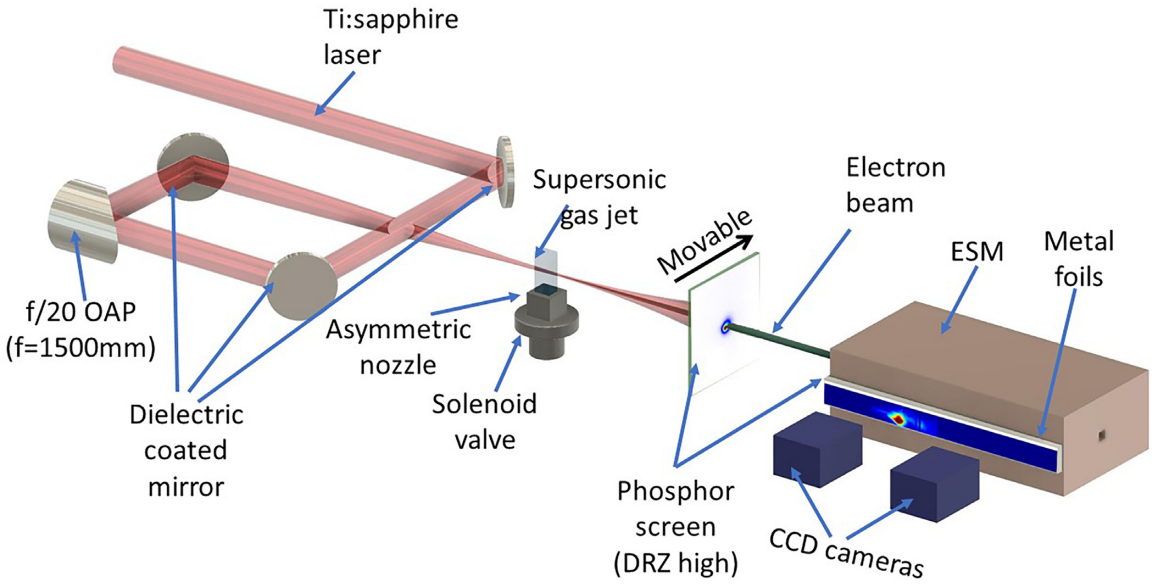

Fig. 2. Schematic setup of LWFA experiment.

angle of collection. The total charge of the electron beam can be calculated using

$$Q = \delta \times \frac{N}{\beta \omega k \eta}, \tag{1}$$

where Q is the total charge of the electron beam. δ is the signal loss from optics, N is the number of photons picked up by the CCD camera, η is the quantum efficiency of the CCD camera, β is the CCD camera gain, ω is the solid angle of the CCD camera and k is the DRZ sensitivity. For this experiment, η equal to 0.92, β equals to 1, ω equals to $3.67 \times 10^{-4} sr$, k equals to $7 \times 10^9\ sr^{-1}\ pC^{-1}$ [34]. δ is estimated to be 0.62 for the optical transport system.

For electron bunch length measurement, a typical single-shot electro-optic (EO) sampling method [35–37] was used. The EO setup in this experiment is the same as the EO experiment recently reported in Ref. [37]. To analyze all LWFA dynamics changes with the density gradient, multidimensional PIC simulations [38] were performed with the modified FPLaser [39] code to provide the exact calculation of light speed in a vacuum. The spatial resolution in the simulation was chosen as $\lambda/24$ in the longitudinal direction and $\lambda/16$ in the transverse direction, and 16 particles per cell. Here λ is the wavelength of the laser pulse. The box size in the longitudinal direction was 150 μm and in the transverse direction was 300 μm. The accuracy of the calculation of laser pulse group velocity in plasma was better than 1%. The linear approximation for the density ramp was used. The laser pulse intensity, the pulse duration and the focus spot size were chosen to be equal to the experimental ones.

3. Result of measurement and calculation

In the LWFA experiment, the gas tank pressure was controlled between 0.3–0.7 Mpa. The maximal plasma electron density in the experiments was estimated to be $N_e \sim (3{-}6) \times 10^{18}\ \mathrm{cm}^{-3}$ for different gas tank pressure. Measurements of accelerated electron energy distribution depending on the gas density down-ramp slope are presented in Fig. 3. When both walls were closed, which corresponds to the flat density distribution shown as the blue line in Fig. 1(e), a rather weak electron signal is observed. That could be a sign of non-efficient electron self-injection or poor emittance of electrons after their acceleration. Their maximal energy is low, less than

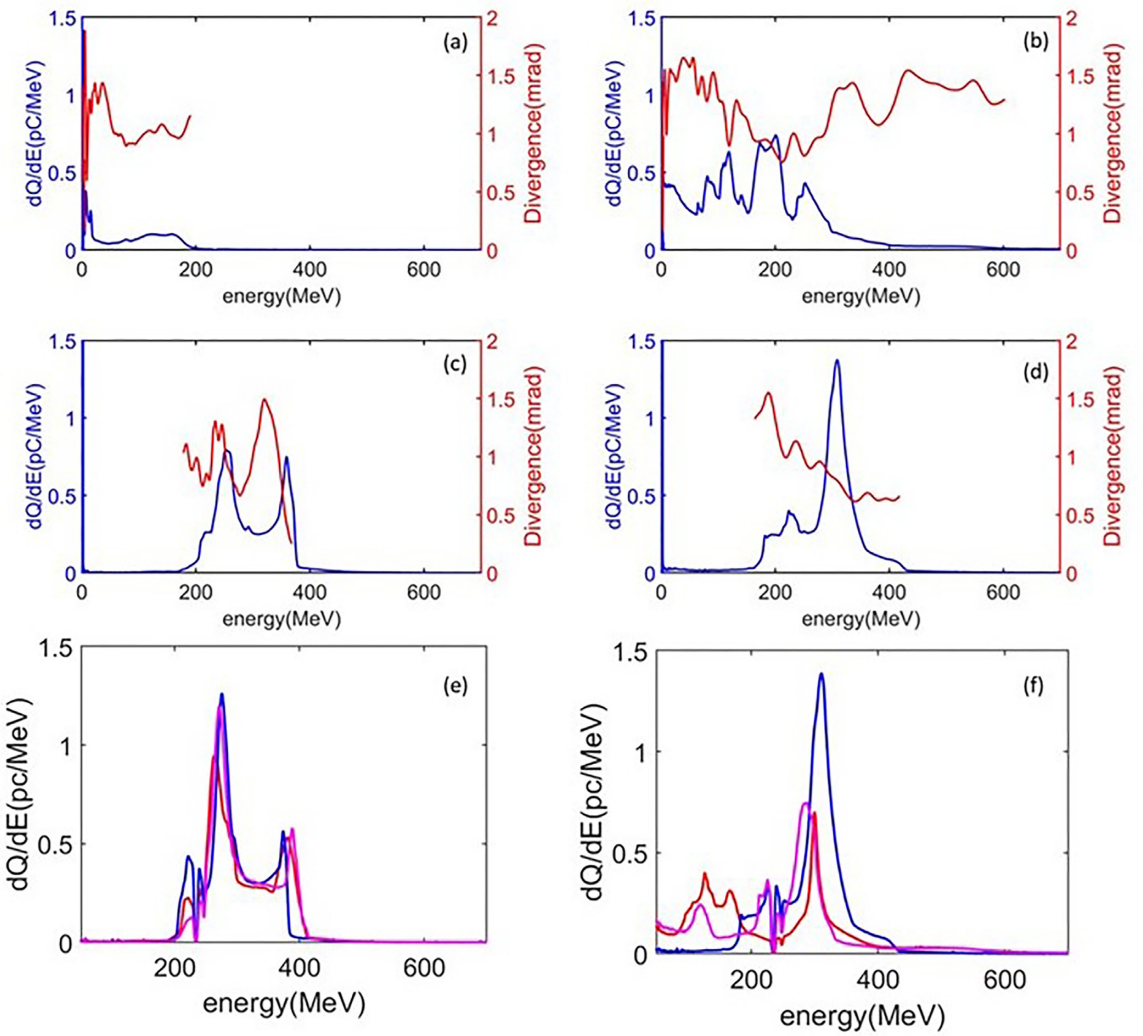

Fig. 3. Measured electron energy for different back wall conditions. (a) full close, total charge 4.9 pC; (b) full open, total charge 50.2 pC; (c) 6 mm open, total charge 38.4 pC; (d) 5 mm open, total charge 51.2 pC. The red lines give the beam divergence (RMS) dependence on energy. (e) Shot-by-shot fluctuation of electron distribution for the experimental condition as in (c); (f) shot-by-shot fluctuation of electron distribution for the experimental condition as in (d).

200 MeV; the bunch charge is also low, < 5 pC (as shown in Fig. 3a). Everything is changed by introducing slope in the gas density profile by opening the wall at the exit end of the gas jet. When the back wall is fully opened, the plasma density gives a down-ramp distribution (see the purple line in Fig. 1e).

A density down ramp results in significant growth of the bunch charge up to 50 pC. However, the electron spectrum exhibits a multi-peak distribution (Fig. 3b). We can observe electron energy peaks at 80 MeV, 125 MeV, 200 MeV and 250 MeV. The variation in the down-ramp slope shows the strong dependency of charge and energy spectrum on the density gradient $N_e/(dN_e/dx)$ even for a small change. As the back wall opens to 6 mm, a double-peak spectrum is observed with a smaller total charge, about 38 pC (Fig. 3c). A further small shift of the back wall, to 5 mm height, drastically changes the results. A mono-energetic electron bunch with its spectrum at 300 MeV with the energy spread around 18% and a total charge of about

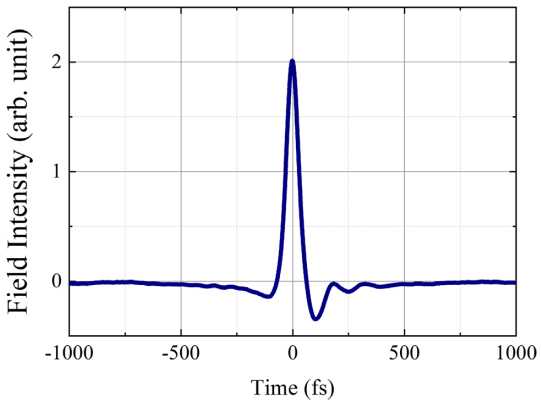

Fig. 4. Typical temporal waveform of the transition radiation induced by the electron bunch accelerated with fully opened nozzle, measured by single-shot EO sampling.

50 pc is generated (Fig. 3d). The reproducibility of these results is illustrated by Figs. 3(e) and 3(f). Typical shot-by-shot fluctuation of the total charge is measured to be about 30% and bunch-pointing stability is about 1.7 mrad. We attribute this fluctuation mostly to the beam-pointing fluctuation. The latter originated from the fluctuation of the laser pulse focus-ability. Owing to the poor pointing stability, electrons from only a limited number of shots enter ESM successfully. However, from the successful shots, ESM data show that the electron beams have similar energy profiles and charges for most cases.

The red lines in Fig. 3 show the measured beam divergence depending on the electron energy. For all cases, the RMS divergence is less than 2 mrad. When a quasi-monoenergetic energy peak appears (Figs. 3c and d), we can observe a smaller divergence <1 mrad, especially in the high energy end of each peak. As shown in Ref. [40], for the second stage acceleration up to GeV energy with reasonable energy of the driving laser pulses, the injected beam charge should be in the range of 10–25 pC and the energy spread 3–10%. This requirement is satisfied in the case of the 5 mm opened back wall nozzle. Upon using a slicing method [19, 20] one can extract 4% energy bunches with a charge of about 12 pC at the mean energy $E = 300$ MeV. This opens up a way to control charge in the staging LWFA. However, processes determining the electron self-injection and their acceleration in such gas targets shall be well understood.

A typical single-shot EO waveform, which is necessary for electron bunch length measurement according to Ref. [37], is shown in Fig. 4. The RMS electron bunch length was estimated to be less than 25 fs. The measurements show a single peak electric field distribution. This indicates that multiple/single injection happens inside one bubble by parametric resonance.

Since there are no steep density gradients in the present experimental set-up, electron self-injection can occur only due to parametric effects [13]. One form of parametric effects is produced by the transverse oscillation of laser waist, which requires a high-density plasma [13]. Another may occur due to a density slope in the case of lower-density plasma. To analyze the process of electron self-injection and dynamics of electron acceleration in laser pulse wake we performed multi-dimensional PIC simulations using the FPlaser code [38,39] and the FBPIC code [41]. To test a possible parametric effect in the case of low-density plasma we consider an ideal case, to exclude other possible injection mechanisms. The maximal plasma density varied from 3×10^{18} to 6×10^{18} cm^{-3}. The linear approximation for the density ramp was used to make the analysis clear. Four cases were considered: uniform plasma of 6 mm in length, plasma

with zero density at the edge, and plasma with an edge density of 0.2 and 0.4 of the maximal density. In the vacuum plasma interface, the density ramp has a linearly increasing profile with a length of 300 μm. In the case of uniform plasma, we observed no self–injection of the electrons in the first bucket for all sets of electron densities. There was electron-self injection in the buckets from 5 to 7 in high-density plasma, $N_e = 6 \times 10^{18}\,\mathrm{cm}^{-3}$ and rather small for low-density case, $N_e = 3 \times 10^{18}\,\mathrm{cm}^{-3}$. However, the geometrical emittance of such electron bunches was too poor. With a small total charge, such small emittance is not likely to makes such bunches observable in the experiments in low-density cases. The case drastically changes with a negative density gradient. In the case of a negative gradient plasma, a laser pulse is "accelerated" since $dv_{gr}/dt \neq 0$, where $v_{gr} = \sqrt{1 - N_e/N_{cr}}$ is the plasma phase velocity and N_{cr} is the critical density for radiation with wavelength λ, while the plasma wake is not due to a retarded effect. In the relativistic reference frame, the equation of electron motion, in the vicinity of $v \sim 0$, can be written in a classical form as

$$\ddot{x} + \omega_{pl}^2 \times \left(1 - \frac{\nabla_l N_e}{N_e} x\right) x = F, \tag{2}$$

where ω_{pl} at $N_e(x)$ is the plasma frequency, $\nabla_l N_e$ is the longitudinal density gradient and F is the driving force.

For an oscillator, one has a typical solution of $x = x_0$:

$$x_0 = A e^{(i\omega_{pl} t)}. \tag{3}$$

We can write equation (2) as

$$\ddot{x} + \omega_{pl}^2 \times (1 + \beta e^{(i\omega_{pl} t)}) x = F, \tag{4}$$

where $\beta = -[(\nabla_l N_e)/N_e] \times A$. We now consider a small deviation of x_1 from x_0, $x = x_0 + x_1$. For this small deviation x_1,we can modify equation (4) as

$$\ddot{x} + \omega_{pl}^2 \times (1 + \beta_0 e^{(i\omega_{pl} t)} + \beta_1 e^{(2i\omega_{pl} t)}) x = F; \tag{5}$$

if we generalize the saturation so that $x = x_0 + x_1 + x_2 + ...$, we can get

$$\ddot{x} + \omega_{pl}^2 \times \left(1 + \sum_{k=1}^{\infty} \beta_k e^{(ik\omega_{pl} t)}\right) x = F. \tag{6}$$

Since $x(t)$ has a periodic structure, Eq.(2) can be easily reduced to the parametric equation [42]. The parametric resonance may result in controllable wave breaking and corresponding electron self-injection [13]. The parameter determining an increment for possible parametric resonance depends not only on the density gradient but also on the density value.

The results of direct simulation clearly demonstrate the existence of the resonance character of the electron self-injection in the case where non-uniformity length far exceeds the plasma wavelength. Again, we observe no electron self-injection in the first bucket in uniform plasma for all considered densities. With the density slope, electron self-injection occurs. In the simulations, the density slope follows the linear relation $N_e(x) = N_e(0)[1 - \alpha x]$, where $N_e(0)$ is the peak density at the entrance edge of the gas-jet, $N_e(x)$ is the final density at the exit of the gas-jet, x is the propagation direction and α is the rate of change of the plasma density along the propagation direction. For $\alpha = (\nabla_l N_e)/N_e = [N_e(0) - N_e(x)]/[xN_e(0)] = 1\mathrm{cm}^{-1}$, the electron self-injection occurs quite late and the final energy of the accelerated electrons is low. This is shown in Fig. 5(a). For $\alpha = 1.33$ we observe a more efficient injection at an earlier stage and, therefore, far higher energy of the accelerated electrons. This is shown in Fig. 5(b), which is similar to the experimental result (see Fig. 3d). The energy spread here is narrow, about 13%.

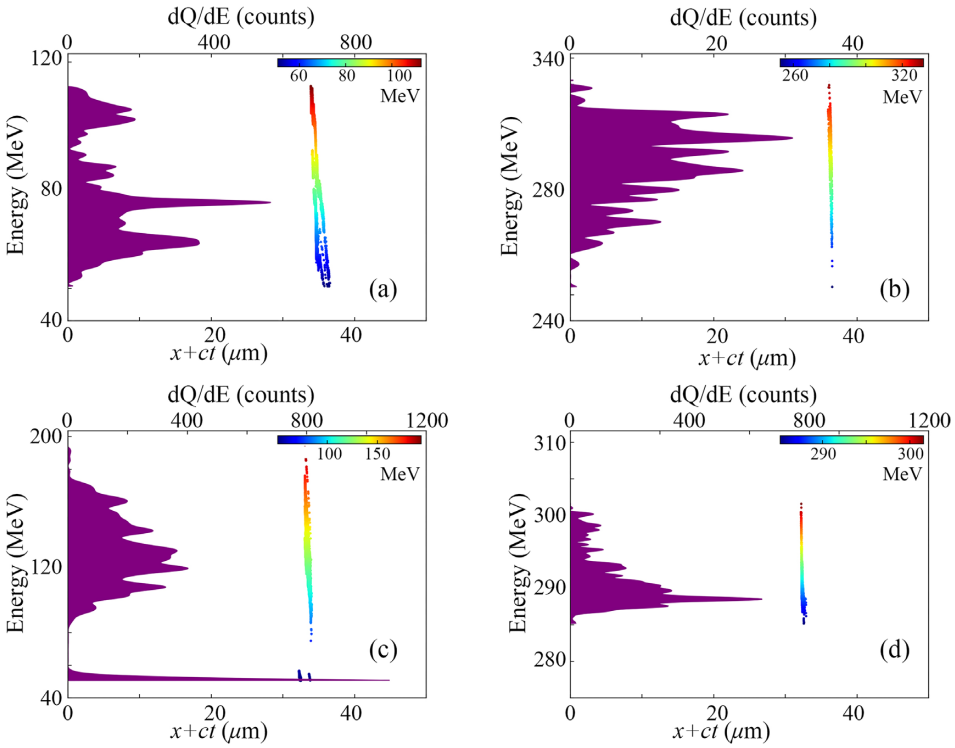

Fig. 5. The energy and phase space distribution for the cases where self-injection occurs in the first bucket. (a) $N_e(0) = 3 \times 10^{18}\,\mathrm{cm}^{-3}$, $N_e(x = 6\,\mathrm{mm}) = 1.2 \times 10^{18}\,\mathrm{cm}^{-3}$ ($\alpha = 1$); (b)$N_e(0) = 3 \times 10^{18}\,\mathrm{cm}^{-3}$, $N_e(x = 6$ mm$) = 6 \times 10^{17}\,\mathrm{cm}^{-3}$ ($\alpha = 1.33$); (c)$N_e(0) = 4.5 \times 10^{18}\,\mathrm{cm}^{-3}$, $N_e(x = 6\,\mathrm{mm}) = 7 \times 10^{17}\,\mathrm{cm}^{-3}$ ($\alpha = 1.33$); (d)$N_e(0) = 6 \times 10^{18}\,\mathrm{cm}^{-3}$, $N_e(x = 4\,\mathrm{mm}) = 0\,\mathrm{cm}^{-3}$ ($\alpha = 2.5$).

Further increase of the density gradient to the maximal $\alpha = 1.67$ gives the negative result; there was no electron self-injection in the first or the second bucket. This is a clear sign of the resonance character of electron self-injection for these conditions.

Next, the peak density in the simulation is increased up to $N_e(0) = 4.5 \times 10^{18}\,\mathrm{cm}^{-3}$. For this peak density, we observed negative results for uniform plasma as well as for plasma density gradient with $\alpha = 1\mathrm{cm}^{-1}$. However, for $\alpha = 1.33$ gradient, electron self-injection occurs but with low final energy of the accelerated electrons. This is shown in Fig. 5(c). With the further increment in the peak density, up to $N_e(0) = 6 \times 10^{18}\mathrm{cm}^{-3}$, all considered cases give negative results: there was no electron self-injection in the first bucket. We attribute this to the decrease of the parametric resonance increments with the density growth as seen in Eq.(2). To verify this phenomenon, we increased the density gradient up to $\alpha = 2.5\,\mathrm{cm}^{-1}$ for the electron density $N_e(0) = 6 \times 10^{18}\,\mathrm{cm}^{-3}$ to fit the increment at lower plasma density. The result is shown in Fig. 5(d). One can see the efficient electron self-injection in this case and the formation of electron bunch with low, 1.7% energy spread at the main energy 287 MeV. This confirms the resonance character of the electron self-injection. However, in the uniform plasma with density $N_e(0) = 6 \times 10^{18}\mathrm{cm}^{-3}$, we observe a rather strong electron self-injection in the rear buckets. The total charge there may be large; however, the emittance of electrons in the rear buckets is far lower compared to the emittance of the electrons generated via parametric resonance, by more than an order of magnitude. We have to note that the resonance self-injection can be multiple [12], which can explain the appearance of peaks in the bunch length measurement.

With the maximal density increase the transverse parametric interaction can become dominant and change the electron self-injection dynamics. In the experiment, the density profile differs from the ideal linear profile; the injection picture may be distinct from that for the linear density slope. To reveal the real dynamic of the electron self-injection and acceleration in the experiment, we made another set of simulations with the gas density distribution obtained with interferometry [red and yellow lines in Fig. 1(e)] and a quasi-3D FBPIC simulation code. The dynamics of electron self-injection and acceleration for cases are presented in Fig. 6 for different density profiles as given in Fig. 1. The parametric character of the electron self-injection is clearly seen in all these cases in the form of single or multiple electron self-injection. However, the selection of the injection mechanism in these cases is difficult because of the complicated character of the density profile.

4. Conclusion

We have investigated the LWFA in longitudinally asymmetric gas jets using gas density and gas density gradient as parameters to examine a possible way to control the total charge of accelerated electrons. 1.2 J on-target laser pulses with 24 fs duration have been exploited as the driving source. In the present experiment, the H_2 gas density was fixed and the density gradient has been varied from zero to the maximal value $\alpha = 1.67\text{cm}^{-1}$. We have also performed multidimensional particle-in-cell simulations with accurate calculation of group velocity of the laser pulses in plasma that allowed us to investigate almost 1 cm propagation length with high accuracy.

The experimental results have demonstrated a clear dependency of the total charge of electron bunch with low emittance on the density gradient. While in uniform plasma the total charge was low, about 4 pC, in plasma with a density gradient it increased up to 50 pC, making such a bunch practical for use in the staging accelerator scheme. The best result has been achieved for a plasma density profile with $\alpha = 1.33\ \text{cm}^{-1}$ for our 50 TW laser system. A bunch with a charge of 51 pC at mean energy $\epsilon = 300$ MeV has been generated at the energy spread of 18% with reasonable reproducibility. A relatively small fluctuation of the total charge and good pointing stability allows the application of this source after the slicing procedure as the cathode in the staging scheme. Easier tuning of the gas density and gas density gradient in the asymmetric gas nozzle makes this device interesting for practical application in LWFA. Our experiment result may not be the best in the world compared to other injection mechanisms, for example, shock injection or ionization injection; however, this paper details the first time an experiment demonstrates electron beam charge control with parametric resonance in the laser propagation direction. We are trying to improve our target so that we can get better experimental results.

2D particle-in-cell simulations carried out have revealed the mechanisms of electron self-injection in plasma targets with α order of unit. The electron self-injection in the first bucket of laser wake is a result of the parametric resonance induced by the acceleration of the laser pulse and, hence, the acceleration of plasma waves in such plasmas. This has been shown via simulation in the density range $N_e = 3 \times 10^{18}$ to $6 \times 10^{18}\,\text{cm}^{-3}$ and density gradient $\alpha = 0$–1.67 and $\alpha = 2.5$. These calculations have also demonstrated the possibility of total charge tuning within the 10–20 pC level to generate well-controlled, low emittance electron bunches with a duration shorter than 30 fs. Quasi-3D simulations with real experiment density profiles confirm the parametric effect on electron self-injection and exhibit a good agreement with the experiment result on the electron acceleration. Since we are working in a highly non-linear

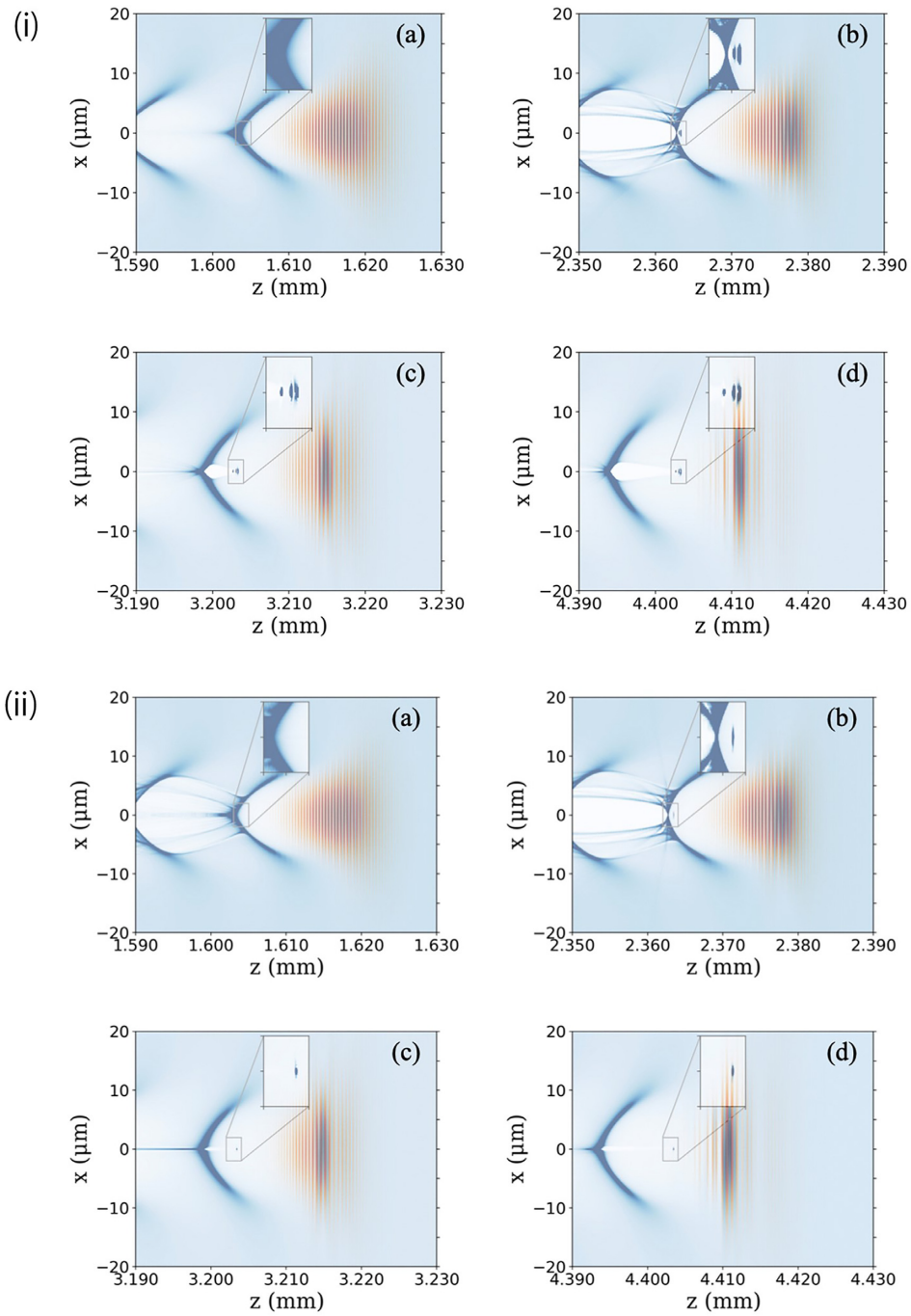

Fig. 6. Plasma density evolution from quasi-3D PIC simulation using density profile obtained from interferometry (i) back wall 6 mm open case [yellow line in Fig. 1(e)]; (ii) back wall 5 mm open case [red line in Fig. 1(e)] at different timings: (a) 5.4 ps, (b) 7.9 ps, (c)10.7 ps and (d) 14.7 ps. The insets show the magnified image of the injected electron beam.

region of laser–plasma interaction, the α value for the best experiment result may change with the laser power. We believe our theory is universal. There will always be an α value that allows us to obtain a quasi-monoenergetic electron beam for different laser power. In the near future, we plan to conduct an experiment with a higher-power laser to confirm our theory.

Acknowledgment

This work was funded by the JST-MIRAI program grant no. JPMJMI17A1, and was partially supported by the ImPACT R&D Program of the Council for Science, Technology and Innovation (Cabinet Office, Government of Japan). We are grateful to the technical teams of Spring-8 Center for their support of the Laser Acceleration Platform. We acknowledge the use of the supercomputer facility of the Cybermedia Centre at Osaka University.

References

[1] P. Gibbon, Short Pulse Laser Interaction with Matter (Imperial College Press, London, 2005), p. 64.
[2] R. J. Shalloo et al., Nature Commun. **11**, 6355 (2020).
[3] J. P. Palastro, J. L. Shaw, P. Franke, D. Ramsey, T. T. Simpson, and D. H. Froula, Phys. Rev. Lett. **124**, 134802 (2020).
[4] C. Joshi, S. Corde, and W. B. Mori, Phys. Plasmas **27**, 070602 (2020).
[5] S. Jalas, M. Kirchen, P. Messner, P. Winkler, L. Hübner, J. Dirkwinkel, M. Schnepp, R. Lehe, and A. R. Maier, Phys. Rev. Lett. **126**, 104801 (2021).
[6] A. J. Gonsalves et al., Phys. Rev. Lett. **122**, 084801 (2019).
[7] M. Reiser, Theory and Design of Charged Particle Beams (Wiley, Weinheim, 1994), p. 507.
[8] E. Esarey, C. B. Schroeder, and W. P. Leemans, Rev. Mod. Phys. **81**, 1229 (2009).
[9] S. V. Bulanov, F. Pegoraro, A. M. Pukhov, and A. S. Sakharov, Phys. Rev. Lett. **78**, 4205 (1997).
[10] A. Pak, K. A. Marsh, S. F. Martins, W. Lu, W. B. Mori, and C. Joshi, Phys. Rev. Lett. **104**, 025003 (2010).
[11] A. Zhidkov, N. Pathak, J. K. Koga, K. Huang, M. Kando, and T. Hosokai, Phys. Rev. Res. **2**, 013216 (2020).
[12] M. Chen, E. Esarey, C. B. Schroeder, C. G. R. Geddes, and W. P. Leemans, Phys. Plasmas **19**, 033101 (2012).
[13] A. Oguchi, A. Zhidkov, K. Takano, E. Hotta, K. Nemoto, and K. Nakajima, Phys. Plasmas **15**, 043102 (2008).
[14] T. Hosokai, A. Zhidkov, A. Yamazaki, Y. Mizuta, M. Uesaka, and R. Kodama, Appl. Phys. Lett. **96**, 121501 (2010).
[15] S. V. Bulanov, T. Zh. Esirkepov, Y. Hayashi, H. Kiriyama, J. K. Koga, H. Kotaki, M. Mori, and M. Kando, J. Plasma Phys. **82**, 905820308 (2016).
[16] A.I. Akhiezer and P.V. Polovin, Soviet Phys. JETP **3**, 696 (1956).
[17] J. M. Dawson, Phys. Rev. **113**, 383 (1959).
[18] A. Pukhov and J. Meyer-ter Vehn, Appl. Phys. B **74**, 355 (2002).
[19] A. Buck et al., Phys. Rev. Lett. **110**, 185006 (2013).
[20] J. Faure, C. Rechatin, A. Norlin, A. Lifschitz, Y. Glinec, and V. Malka, Nature **444**, 737 (2006).
[21] Y. Sakai et al., Phys. Rev. Accel. Beams **21**, 101301 (2018).
[22] Z. Jin, H. Nakamura, Y. Pathak, N.and Sakai, A. Zhidkov, K. Sueda, R. Kodama, and T. Hosokai, Sci. Rep. **9**, 20045 (2019).
[23] K. Schmid, A. Buck, C. M. S. Sears, J. M. Mikhailova, R. Tautz, D. Herrmann, M. Geissler, F. Krausz, and L. Veisz, Phys. Rev. ST Accel. Beams **13**, 091301 (2010).
[24] Z. Zhang et al., New J. Phys. **17**, 103011 (2015).
[25] S. Bulanov, N. Naumova, F. Pegoraro, and J. Sakai, Phys. Rev. E **58**, R5257 (1998).
[26] P. Tomassini, M. Galimberti, A. Giulietti, D. Giulietti, L. A. Gizzi, L. Labate, and F. Pegoraro, Phys. Rev. ST Accel. Beams **6**, 121301 (2003).
[27] A. V. Brantov, T. Zh. Esirkepov, M. Kando, H. Kotaki, V. Yu. Bychenkov, and S. V. Bulanov, Phys. Plasmas **15**, 073111 (2008).
[28] G. Golovin et al., Nucl. Instr. Method. Phys. Res. A **830**, 375 (2016).
[29] J. D. Anderson, , Jr., Fundamentals of Aerodynamics (McGraw-Hill, New York, 2006), p. 669.
[30] J. D. Anderson, , Jr., Modern Compressible Flow: With Historical Perspective (McGraw-Hill, New York, 2002), p. 147.
[31] H. Kotaki et al., Phys. Plasmas **9**, 1392 (2002).
[32] J. R. Rumble, CRC Handbook of Chemistry and Physics, (CRC Press, Boca Raton, FL, 2021), 102 ed., p.6–21.

[33] D. Strickland and G. Mourou, Opt. Commun. **56**, 219 (1985).
[34] Y. C. Wu, B. Zhu, K. G. Dong, Y. H. Yan, and Y. Q. Gu, Rev. Sci. Instr. **83**,026101 (2012).
[35] J. Shan, A. S. Weling, E. Knoesel, L. Bartels, M. Bonn, A. Nahata, G. A. Reider, and F. Heinz, Opt. Lett. **25**, 426 (2000).
[36] K. Huang, T. Esirkepov, J. K. Koga, H. Kotaki, M. Mori, Y. Hayashi, N. Nakanii, S. V. Bulanov, and M. Kando, Sci. Rep. **8**, 2938 (2018).
[37] K. Huang, Z. Jin, N. Nakanii, T. Hosokai, and M. I. Kando, Appl. Phys. Exp. **15**, 036001 (2022).
[38] A. Zhidkov, J. Koga, T. Hosokai, K. Kinoshita, and M. Uesaka, Phys. Plasmas **11**, 5379 (2004).
[39] N. Pathak, A. Zhidkov, and T. Hosokai, Phys. Lett. A **425**, 127873 (2022).
[40] N. Pathak, A. Zhidkov, Y. Sakai, Z. Jin, and T. Hosokai, Phys. Plasmas **27**, 033106 (2020).
[41] R. Lehe, M. Kirchen, I. A. Andriyash, B. B. Godfrey, and J.-L. Vay, Comp. Phys. Commun. **203**, 66 (2016).
[42] E. M. Lifshitz and L. D. Landau, Mechanics (Pergamon Press, London, 1960), p. 80.